Received 8 February 2023, accepted 1 March 2023, date of publication 6 March 2023, date of current version 10 March 2023.

Digital Object Identifier 10.1109/ACCESS.2023.3253556

APPLIED RESEARCH

A High Gain Deployable L/S Band Conical Helix Antenna Integrated With Optical System for Earth Observation CubeSats

NURSULTAN MEIRAMBEKULY[1], BEIBIT A. KARIBAYEV[1], TIMUR A. NAMAZBAYEV[1], GULAMA-GARIP ALISHER E. IBRAYEV[1], SABYR O. ORYNBASSAR[2], SAMSONENKO ANATOLIY IVANOVICH[3], AND AMIRKHAN A. TEMIRBAYEV[1]

[1]Al-Farabi Kazakh National University, Almaty 050038, Kazakhstan
[2]International Taraz Innovative Institute named after Sherkhan Murtaza, Taraz 080000, Kazakhstan
[3]SLLP "Institute of Space Technique and Technology," Almaty 050061, Kazakhstan

Corresponding author: Amirkhan A. Temirbayev (amirkhant@gmail.com)

This research has been funded by the Science Committee of the Ministry of Science and Higher Education of the Republic of Kazakhstan (Grant No. AP09057984).

ABSTRACT In this study, a new spiral dual-band antenna integrated with an optical system for a small CubeSat spacecraft was proposed. It is challenging to design an antenna with a limited space on a CubeSat platform. To improve the space utilization, an antenna was designed based on the concept of not occupying the sides of the CubeSat. A feature of the proposed antenna system is its compactness, dual-band operation in the L- and S-bands, and possibility of integration with spacecraft cameras. As a result of the study, reflection coefficients of −18 dB and −23 dB and gain of 6.8 dBi and 7.4 dBi, respectively, were achieved at resonant frequencies of 1.7 GHz and 2.45 GHz. The conical shape of the spiral antenna allows the optical system to increase the coverage area, and a simple deployment system with feedback ensures the mission safety. These properties make the proposed antenna suitable for CubeSat systems.

INDEX TERMS CubeSat antenna, dual-band antenna, earth observation, helix antenna.

I. INTRODUCTION

At present, the use of small spacecraft (SS) and their constellations is gaining increasing popularity for solving urgent problems related to the study of Earth from space [1], [2]. SSs have a relatively smaller mass than large spacecraft (LS); they undergo the stages of the life cycle faster, such as design, construction, manufacturing, and testing, and require significantly lower costs.

A Cubesat is a standard for SS proposed at the end of the last century [3]. Due to their small size, such ''micro'' and ''nano'' satellites are often launched on rockets, which, according to the plan, put other, more bulky spacecrafts into orbit [4]. This greatly reduces the cost of obtaining a modern satellite with a relatively wider functionality. A feature of CubeSats is the fixed dimensions that change multiple times; that is, a 1U Cubesat (unit) is a space cube of 10 × 10 × 10 cm, and 2U is two cubes (10 × 10 × 20 cm). 1U, 3U, and 6U

were the three most common and relevant modifications respectively. Nanosatellites have a wide range of applications, from interplanetary missions to space observations and communications [5], [6], [7]. A special place is occupied by remote sensing of Earth (ERS) [8], [9], [10], [11].

Despite their effectiveness, the small size of CubeSats has forced scientists to seek new ways to solve the existing problems. It is difficult to insert tools, appliances, or other equipment into a small apparatus Therefore, the development of new solutions for circuits and the miniaturization of on-board systems, modules, and their optimal locations, including antenna devices, make it possible to effectively use the limited space on the surface [12], [13], [14].

Various types of antennas, depending on the mission, capabilities of the spacecraft, and frequency band, are used for transmitting and receiving data (Tracking, Telemetry and Control (TT&C), image, etc.) in many CubeSats,

The associate editor coordinating the review of this manuscript and approving it for publication was Hassan Tariq Chattha.

in operation, or under design. Most of the CubeSat missions used VHF and UHF radio frequency (RF) communications with typical data rates of 1.2 and 9.6 Kbps for both telemetry and payload data transmission. As a rule, in the VHF and UHF bands, wire, tape monopole and dipole antennas are widely used because of the simplicity of their manufacture [15], [16], [17], [18]. The typical monopole or dipole sizes of these bands were larger than those on the surface of the CubeSat. In [19], to achieve compact dimensions, a curved meander line located on one side of the substrate was used for the UHF antenna and a deployable design was used for the VHF antenna. In [20], a simplified system was developed using a dual-band VHF/UHF antenna instead of the standard dual-antenna system commonly used in CubeSats. Even though VHF and UHF antennas are used in more than 50 % of launched nanosatellite missions [21], they have a fundamental limiting factor related with downlink speeds. Therefore, today there is a necessity to switch to higher frequency ranges (L, S, X, Ka bands) that require appropriate antennas [22].

Patch antennas, which mainly operate in the L- and S-bands, are the second most popular because of their low profile, light weight, and lack of additional deployment mechanisms [23], [24], [25], [26], [27], [28], [29], [30]. The features of patch antennas have been listed, considered, and noted in previous review articles [16], [17], [22], [31]. Although the gains in patch antennas are relatively high compared to wire antennas, they are limited owing to their structural features and manufacturing technology [32]. In the same review paper [32], statistical data indicated that helical antennas allow for even more gain within the VHF to S-bands compared to patch/planar antennas and can be easily assembled and deployed. In [33], conical log spiral and quadrifilar helix antennas (QHA) were used for the UHF band, as well as a deployment mechanism that includes spiral pantograph and origami models with a Z-fold configuration. The study [34] considered the 1U CubeSat mission, which requires an antenna for bands such as L1, L2, and E1, and a microwave radiometry band (1400–1427 MHz) with a gain of 8-12 dB. After a review analysis, the authors noted that among the practically used antennas, the helical antenna is the most suitable. The papers [35], [36] present and test a mechanical deployment solution from a stowed configuration of the same antenna, which allows the antenna to be deployed from 25.5 mm to 506 mm. In [37] the miniaturization of a QHA for space applications (TT&C) in the UHF band was described. Previous studies [38], [39] have described the principles of the mechanisms of the existing deployable UHF helical antennas.

Despite their features and functionality, the patch and helical antennas discussed above have not been integrated into their designs with other payloads. To date, remote sensing nanosatellites have used separate locations on the surface of antennas and at the base of the lenses of optical instruments [40], [41], [42], [43], [44], [45], [46], [47], [48], [49]. In the 3U nanosatellite Phoenix, built to study the urban heat island (UHI) using thermal infrared (IR) remote sensing, the lens base and S-band patch antenna are located on different sides of a cube [40]. Such an approach to the arrangement of components requires the physical reorientation of the spacecraft during the transmission/reception of data. The 6U Cubesat EIVE considered in [41] has no integrated payloads, such as S- and E-band antennas and a 4 K camera on its board. The S-band antennas of the Earth observation nanosatellites Aalto-1 and GOMX-4 are also located separately from other subsystems, such as the Attitude Determination and Control System (ADCS), Spectral Imager (AaSI) and the NanoCam optical camera [42], [43], [44], occupying a usable area for solar panels. The 3U nanosatellite RITA considered in [45] contains an L-band antenna array and a hyperspectral camera (for vegetation analysis), which are also located separately on its board. Thus, it can be seen that the integration of the antenna system with remote sensing equipment for optimization purposes is rarely practiced. Only [50] and our previous paper [51] showed the combined location of a patch antenna and an optical camera. However, as noted above, patch antennas are only well suited for LEO CubeSats owing to their directional properties and gain value (relatively low). There is a need for a more directional antenna with relatively high gains in cases of missions outside this orbit or where higher data rate links are required.

In this paper, we propose the L- and S-band cone helical antenna integrated with an optical camera. A conical shape was selected to fit the viewing angle of the camera and provide coverage over a larger area. Unlike the traditional cylindrical shape, this does not create a static visual hindrance during shooting. Thus, in this type of integration, each subsystem – the antenna and the optical equipment for Earth survey work independently of each other, although they are structurally combined.

II. MATERIALS AND METHODS

The proposed L- and S-band spiral antenna is intended for use in CubeSat nanosatellites used in remote sensing of the Earth and has a round window for the lens of optical equipment. The basic configurations and geometric parameters of the proposed antenna are shown in Fig. 1.

The proposed spiral antenna was simulated using CST Microwave Studio (2018). A one-sided FR-4 (ε=4.3) material with dimensions of 100 mm × 100 mm × 3 mm, with a window for the optical system in the middle with a diameter of D = 36 mm, and with cutouts at the corners repeating the elevations of the end side of the CubeSat case with dimensions of 9 mm × 9 mm were used as antenna substrate. Brass (91%) with a thickness of d=1 mm and the SMA vertical mount connector as the power port were chosen as the spiral material. In this case, the spiral has the shape of a cone, that expands as the height increases. The minimum and maximum radii of the spiral circles were r_1 and r_2, respectively. The power to the antenna emitter is supplied at point P

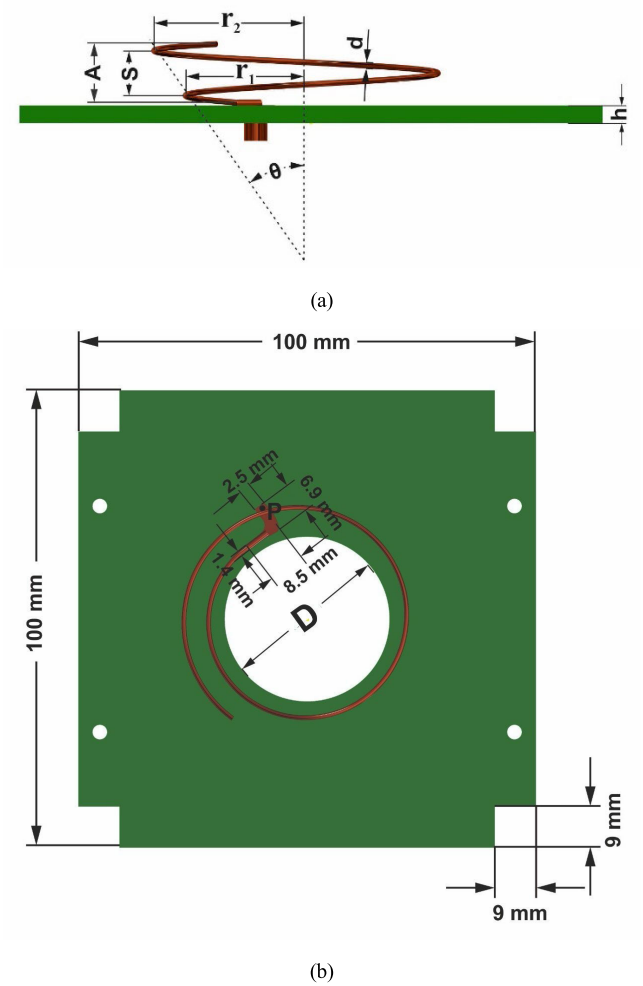

FIGURE 1. The model of the proposed spiral antenna, (a) – side view, (b) – top view.

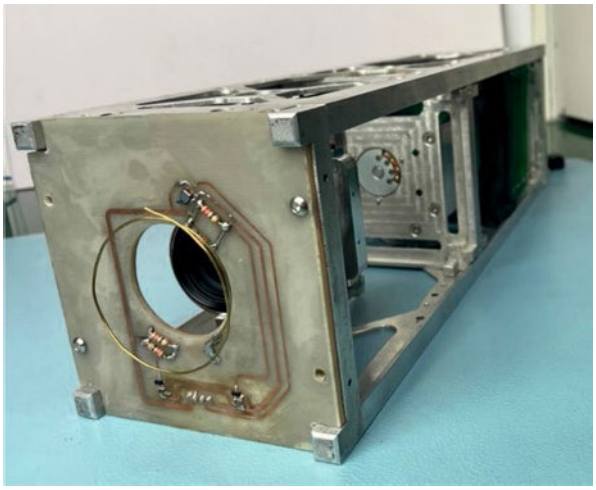

FIGURE 2. A prototype antenna attached to a 3U CubeSat body.

and transmitted to the spiral via an L-shaped microstrip line with overall dimensions of 6.9 mm x 8.5 mm (Fig. 1 (b)). The antenna was designed to be attached to the end side of a nanosatellite in the same direction as that of remote sensing camera (Fig. 2).

Simultaneously, the research team chose a compact low-turn version instead of a multi-turn (N>3) spiral because of the peculiarities of the antenna configuration, where the antenna with a helical receiver was located outside the end part of the nanosatellite, without taking up space inside the spacecraft. At the same time, the assembled antenna must not be higher than the "legs" of the CubeSat located at the four corners of the end part. Fig. 3 shows the dimensions of the assembled spiral antenna, where the height of the antenna is 5.5 mm and does not exceed the height of the "legs" (7 mm).

Calculations of the resonant frequencies of the proposed antenna were carried out for the axial mode of radiation, where the circumference of the spiral antenna is $C \approx \lambda$ [52]. Due to the presence of two turns of unequal size, two resonant frequencies were formed. The radiation of the first resonant frequency f_1 of the antenna is related to the total physical length of the spiral and it is determined as follows:

$$f_1 = \frac{c}{C_1 + \frac{C_2}{3}} = \frac{c}{2\pi r_1 + \frac{2\pi r_2}{3}}, \tag{1}$$

where c is the speed of light, C_1, $C_2$are the circumferences of the small and large turns, respectively, r_1, r_2 are the radii of the small and large turns, respectively (Fig. 1(a)). Here, C_2 is divided by 3, since the length of the second turn is 1/3 of the whole circle. The frequency of the second resonance f_2 is determined accordingly by the formula:

$$f_2 = \frac{c}{C_1} = \frac{c}{2\pi r_1}. \tag{2}$$

As a result of calculations according to formulas (1) and (2), the resonant frequencies $f_1 \approx 1.7$ GHz and $f_2 \approx 2.45$GHz were determined.

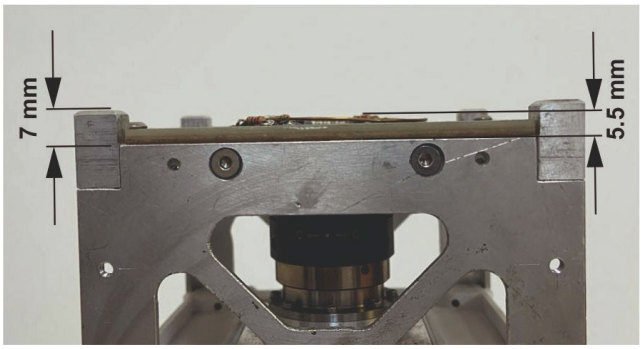

FIGURE 3. Dimensions of the assembled antenna.

Fig. 4 shows the dependences of the resonant frequencies on the geometric parameters of the antenna, as a result of which the most optimal parameters were selected (Table 1). According to Fig. 4(a), as the distance between the turns of the spiral S increases, the resonant frequencies shift downward. However, there was a less obvious shift in the first resonant frequency. In the case of an increase in the angle of expansion of the spiral cone θ (Fig. 4(b)), both resonant

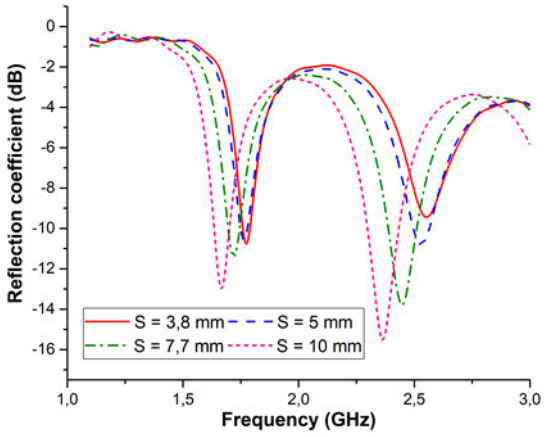

(a)

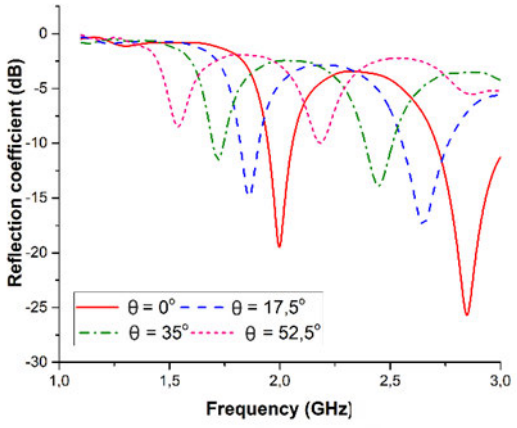

(b)

FIGURE 4. Optimization of antenna parameters, (a) - the effect of the length of the distance between the turns of the spiral S on the resonant frequencies, (b) - influence of the spiral expansion angle Θ on resonant frequencies.

frequencies exhibited an even-dimensional downward shift with a deterioration in the reflection coefficient.

The conical shape of the spiral antenna corresponded to the viewing angle of the camera. The width of the swath (S) available on the market in (many) optical cameras and multispectral imagers ranges from 5 to 195 km for height H=500 km [53], [54]. With such parameters, the values of scan angle (α) lie in the range from 1° to 30°, which can be calculated using the following formula (3) [55]:

$$S = 2 \cdot H \cdot \tan(\frac{\alpha}{2}). \tag{3}$$

For example, when shooting a NanoCam C1U [56] with a focal distances of 35/70 mm, the scan angle is 63/34°, respectively. Thus, the opening angle of the proposed antenna, which is equal to 70°, exceeds the viewing angle of existing optical cameras, thereby does not create visual interference during scanning.

TABLE 1. The antenna design parameters.

Parameters	Explanation (unit)	Value
A	Total height of the spiral (mm)	10
S	Distance between turns (mm)	7.7
d	Wire diameter (mm)	1
θ	The angle of inclination (°)	35
h	Substrate thickness (mm)	3
N	Number of turns	1.33
r_1	The minimum radius of the spiral (mm)	19.5
r_2	The maximum radius of the spiral (mm)	26.5

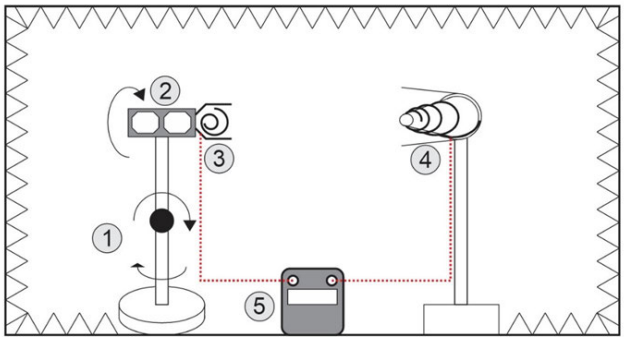

FIGURE 5. Block diagram of the measuring complex, 1 – rotary system, 2 – CubeSat frame, 3 – proposed antenna, 4 – special measuring antenna, 5 – analyzer N9915A.

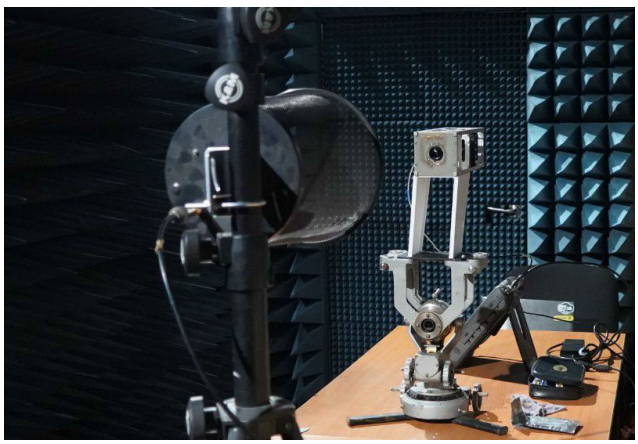

FIGURE 6. The appearance of the measuring complex.

MS46121A vector analyzer, RF signal generator NI PXIe-1065, and the spectrum analyzer Agilent N9340B were used to study S_{11} parameter, Axial Ratio (AR) and Gain of the antenna. Physical measurements were performed in an anechoic chamber to determine the antenna characteristics. Fig. 5 and Fig. 6 show the block diagram and the measuring complex to obtain radiation pattern respectively. A 3U CubeSat

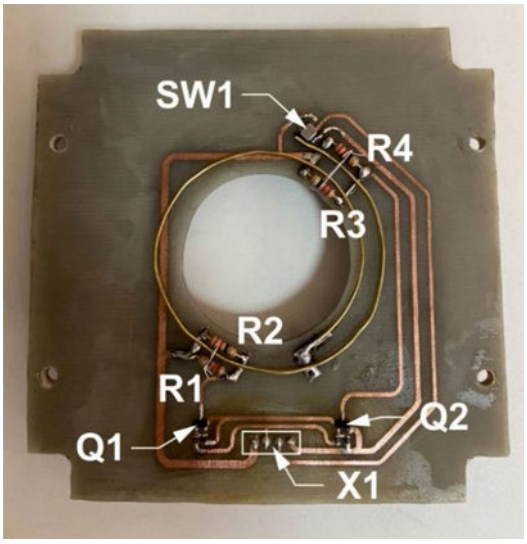

(a)

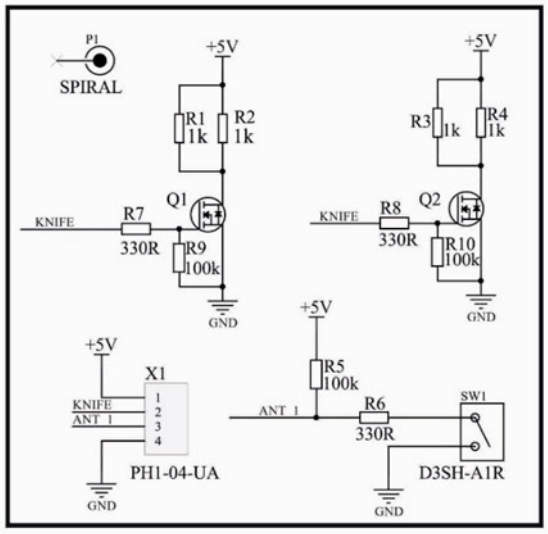

(b)

FIGURE 7. The antenna in the assembled state (a) and electrical circuit of the deployment system (b).

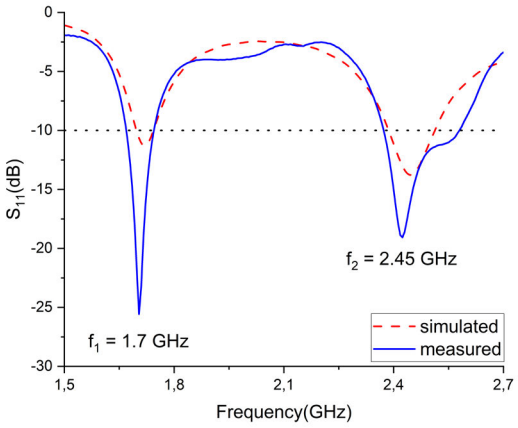

FIGURE 8. Results of modeling (dashed line) and measurements (full line) of the antenna's reflection coefficient.

frame "2" was attached to the upper part of the rotary system "1" along with the antenna "3". By installing them in this way, we also aimed to determine the effect of the metal body of the spacecraft on the antenna pattern. A special measuring antenna "4" with known characteristics was used. The height $\mathbf{h_0}$ of both antennas from the ground was 1 meter. If we consider the condition $\mathbf{h_0} \gg \boldsymbol{\lambda}$, then this height is sufficient to minimize the influence of reflective metals. The data were measured and recorded using the analyzer N9915A "5" in 5-degree increments using a rotary system. The distance between the antennas R is 1 meter, which fully satisfies the condition of the far field ($\mathbf{R} \geq \frac{\mathbf{2L^2}}{\boldsymbol{\lambda}}$, where L is the maximum overall size of the antenna) for resonant frequencies of 1.7 GHz and 2.45 GHz.

To study the gain (G) of the antenna, a method using three antennas was applied [57], where there are:

a) The proposed antenna;

b) An antenna with a known Reference Gain (G_{Ref}) indicator operating at a given frequency;

c) The third antenna operates within a given range (it can be used with unknown gain).

At the first measurement, considering the boundary conditions of the study, a signal is transmitted using an antenna (b) and received using the antenna (c). The power level of received signal is designated as the Reference Level (L_{Ref}). Subsequently, without changing the conditions, the cables, connectors/adapters, and antenna (b) were changed to antenna (a), and the operation was repeated. The received power level of signal was recorded as the Measured Level (L_{Meas}). Using the obtained data, the antenna gain is calculated as follows:

$$G\,(dB) = G_{Ref} + \left(L_{Meas} - L_{Ref}\right). \tag{4}$$

To study the polarization of the antenna, a method for measuring the axial ratio of antennas based on the rotation of the polarization was used [58].

A. ANTENNA DEPLOYMENT SYSTEM

Owing to configuration features of the proposed antenna, in which the emitter is a spiral of a certain height, it does not fit the height of the legs of the end part of the nanosatellite when opened. A spacecraft must be assembled before it is separates from the launch container. A deployment system was developed using the Altium Designer software environment. The features of this assembly/disclosure system include the simplicity of implementation and sufficient design reliability. The spiral antenna was loaded in a specific area on the board between the output heating resistors. Since the spiral antenna structure has the property of a tension spring, it must be fixed with a nylon thread around the spiral wire and heating resistors.

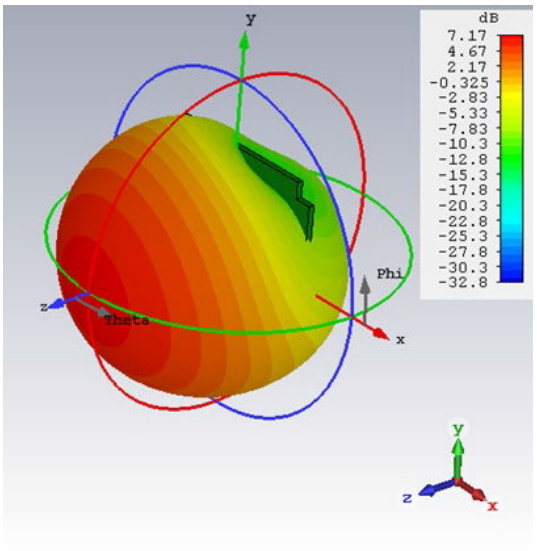

(a)

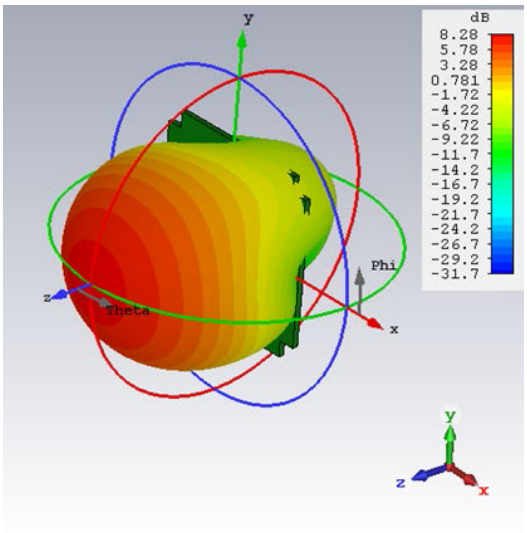

(b)

FIGURE 9. The results of modeling 3D antenna radiation patterns at frequencies of 1.7 GHz (a) and 2.45 GHz (b).

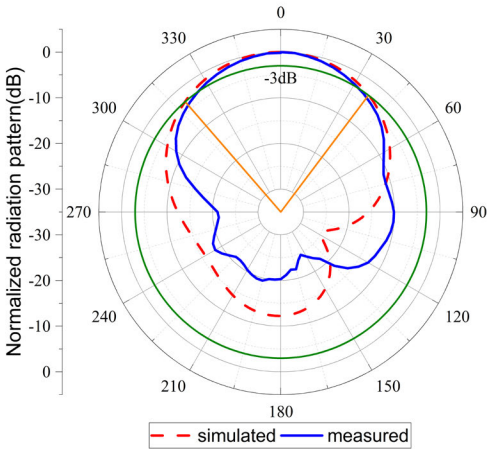

(a)

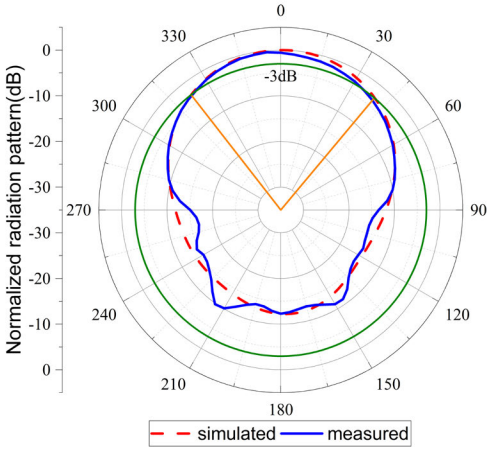

(b)

FIGURE 10. Results of simulation (dashed red line) and measurements (full blue line) of E-plane (a) and H-plane (b) of the 2D radiation pattern of the antenna at a frequency of 1.7 GHz.

The heating resistors serve simultaneously as a starting element for opening the antenna and guiding for proper folding, and between the heating resistors, there is a hole for a reference point for tightening the antenna. When the antenna was tightened and folded correctly, the end of the spiral was mated to a special end cap (SW1) (Fig. 7 (a)), which provided a feedback signal when opening. To open the antenna, power was supplied to the resistors, and the resistor in turn ignited and cut the nylon thread by fixing the antenna. Subsequently, owing to the elasticity of the spiral, it opens, and the end cap signals the success or failure of the disclosure. If the antenna is not opened in the first attempt, the operation can be repeated. The electrical circuit of the disclosure system is shown in Fig.7(b). The resistors (R1, R2, R3, and R4) were heated by opening the gate of the n-channel field-effect transistors (Q1, Q2) that closed the circuit to the ground. The heating control signal was supplied via a bayonet connector with a pitch of 2.54 mm (X1). Output resistors with a nominal value of 22 Ohm and dissipation power of 0.25 W were selected as the heating resistors, and DMG2302 (Q1, Q2) field-effect transistors in the SOT23 housing for the SMD mounting were also selected. D3SH-A1R was used as a side-locking end cap (SW1). All other passive radio components were selected for SMD mounting using a 0603 housing.

III. RESULTS

This section describes the results of the measurements and the research on the main characteristics of the prototype antenna.

Fig. 8 shows the results of modeling and physical measurement of parameter S_{11}, according to which, in the selected area, the antenna has two resonances with center frequencies

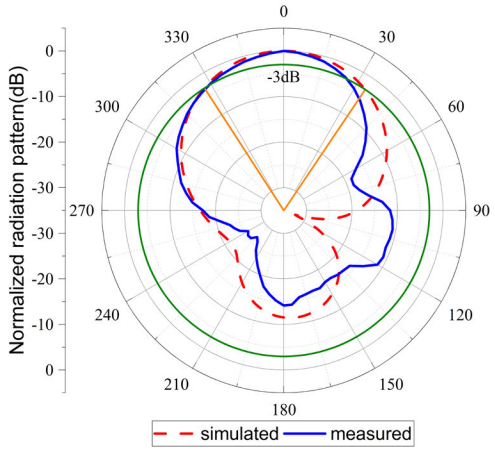

(a)

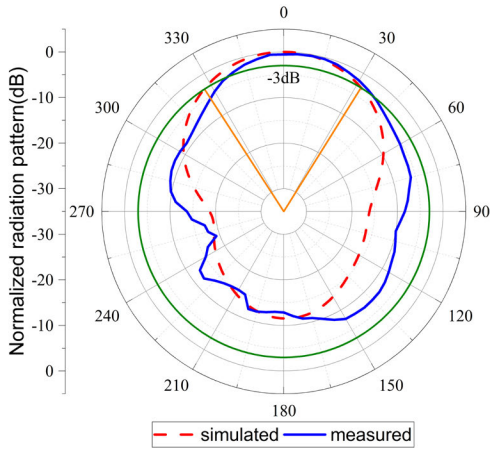

(b)

FIGURE 11. Results of simulation (dashed red line) and measurements (full blue line) of E-plane (a) and H-plane (b) of the 2D radiation pattern of the antenna at a frequency of 2.45 GHz.

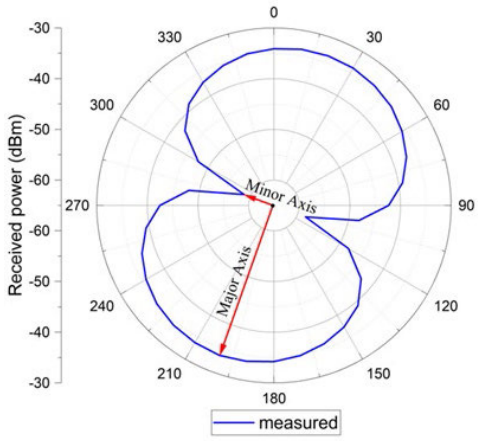

(a)

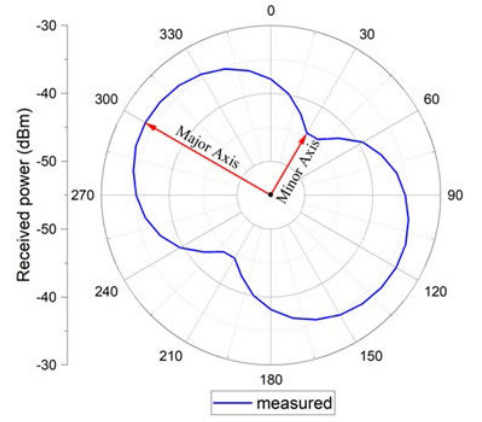

(b)

FIGURE 12. Polarization diagrams in resonant frequencies of 1.7GHz (a) and 2.45 GHz (b).

$f_1 = 1.7$ GHz and $f_2 = 2.45$ GHz. If at a frequency of 1.7 GHz the reflection coefficient is about -25 dB, then at a frequency of 2.45 GHz it shows about -19 dB, with the achievement of -10 dB with impedance bandwidths of 80 MHz (1660 MHz-1740 MHz) and 210 MHz (2390 MHz – 2600 MHz), respectively. The computer simulation and measurement data were consistent except for a small offset at the first resonant frequency.

Fig. 9 shows the results of modeling a 3D antenna pattern at frequencies of 1.7 GHz and 2.45 GHz. According to the figures, the maximum radiation is directed along the Z-axis and shows the maximum gain values of 7.17 dBi and 8.28 dBi at the first and second resonant frequencies, respectively. Fig.10 shows the 2D radiation patterns of the E-plane (a) and H-plan (b) at a frequency of 1.7 GHz. According to the figures, the direction of the maximum radiation coincides with the direction of sight with an aperture of -3 dB at approximately 70° in the E and H-planes, respectively. As a result of the measurement at the selected frequency, the maximum gain of 6.8 dBi was achieved. Fig. 11 shows 2D radiation pattern on the E-plane (a) and H-plane (b) at a frequency of 2.45 GHz. At this frequency, the -3 dB aperture has a width of approximately 60°. In addition, a maximum gain of 7.4 dBi was achieved at this frequency. At the same time, there is a slight discrepancy between the simulation and measured results. This is since during physical measurements, the antenna was integrated with the CubeSat body (Fig. 6), which led to some small changes in the shape of the radiation pattern. At the same time, the shapes of the main lobes coincide. The results of the modeling and measurements at both frequencies were in good agreement.

Fig. 12 shows polarization diagrams of the resonant frequencies. The red arrows show the components of the amplitudes, that is major and minor axes in orthogonal directions. Axial ratio was found, as a result of which the types of polarization were determined. For the first resonance with

TABLE 2. Comparative characteristics of antennas.

Reference	Type of antenna	Size (in the deployed state)	Resonant frequencies (MHz)	Measured peak gain (dBi)
[23]	patch	38.5 mm ×43.5 mm × 2.1 mm	2060	5.5
[25]	patch	96 mm × 96 mm × 2.1 mm	2450	3.7
[34]	Helix	87 mm × 87 mm × 27.5 mm (515 mm)	1575	11.15
[51]	patch	100 mm × 100 mm × 6.8 mm	2010 2200	2 4
Proposed antenna	Helix	100 mm × 100 mm × 5.5 mm (13 mm)	1690 2450	6.8 7.4

a frequency of 1.7 GHz, the AR values was 25 dB, and for the second resonance, it was 10 dB. From these data, as well as from the shape and angle of the polarization diagrams, at the first resonance, the antenna has a polarization closer to linear (Fig. 12(a)), since its orthogonal components have a large difference in amplitudes, and at the second resonance the type of polarization is closer to circular (Fig. 12(b)). The presence of such types of polarization is explained by the fact that the antenna has different radii at the turns and has a small number of turns (N<3), which does not allow to obtain circular polarizations in both bands.

The Table 2 shows the results of comparing the characteristics of the proposed antenna and some of the antennas from the references.

According to Table 2, the proposed antenna is inferior in compactness to the patch antennas [23], [25], [51], but it has a higher gain. In addition, the proposed antenna, along with the antenna from [51], has a dual-band gain compared to the other considered antenna. Compared to antenna system in [34], the proposed antenna is more compact and can be integrated with the CubeSat camera, although it has a slightly lower gain. Given these characteristics, it can be assumed that the proposed antenna can be used in CubeSat spacecraft for remote sensing missions.

IV. CONCLUSION

In this study, a compact, dual-band helical spiral antenna integrated with a CubeSat optical system for remote sensing missions was investigated. A prototype of the designed antenna system has been fabricated and measured. The simulated results and measured results show good agreement. A distinctive feature of the antenna is its compactness in comparison to existing analogs. The antenna can be attached to the end side of the nanosatellite together with the camera, without using additional space in the side area, thus providing space for the solar panels or other equipments. Given the limited size of CubeSats, the antenna that we offer allows for efficient use of the surface. The antenna operates in the L- and S-bands, where the reflection coefficient is much lower than −10 dB, VSWR is lower than 2, and gains of 6.8 dBi and 7.4 dBi are achieved, respectively. In summary, the dual-band deployable antenna system proposed in this study, which demonstrate excellent performance and reliability, as well as simplicity of manufacture and deployment system, compact dimensions, can be used in similar Remote Sensing CubeSat applications. In future we are going to do space environment tests, such as vibration, thermal vacuum cycling, and thermal shock of proposed antenna. In addition, the scientific group plans to develop antenna arrays based on the proposed configuration in the future.

REFERENCES

[1] T. Villela, C. A. Costa, A. M. Brandão, F. T. Bueno, and R. Leonardi, "Towards the thousandth CubeSat: A statistical overview," *Int. J. Aerosp. Eng.*, vol. 2019, Jan. 2019, Art. no. 5063145, doi: 10.1155/2019/5063145.

[2] N. Saeed, A. Elzanaty, H. Almorad, H. Dahrouj, T. Y. Al-Naffouri, and M.-S. Alouini, "CubeSat communications: Recent advances and future challenges," *IEEE Commun. Surveys Tuts.*, vol. 22, no. 3, pp. 1839–1862, 3rd Quart., 2020, doi: 10.1109/COMST.2020.2990499.

[3] J. Puig-Suari, C. Turner, and W. Ahlgren, "Development of the standard CubeSat deployer and a CubeSat class PicoSatellite," in *Proc. IEEE Aerosp. Conf.*, vol. 1, Mar. 2001, pp. 1–347, doi: 10.1109/AERO.2001.931726.

[4] T. Wekerle, J. B. Pessoa, and L. Costa, "Status and trends of smallsats and their launch vehicles—An up-to-date review," *J. Aerosp. Technol. Manage.*, vol. 9, no. 3, pp. 269–286, 2017, doi: 10.5028/jatm.v9i3.853.

[5] Y. Duann, L. C. Chang, C.-K. Chao, Y.-C. Chiu, R. Tsai-Lin, T.-Y. Tai, W.-H. Luo, C.-T. Liao, H.-T. Liu, C.-J. Chung, R. Duann, C.-L. Kuo, J.-Y. Liu, Z.-M. Yang, G. F. Gacal, A. Chandran, H. Priyardarshan, A. Verma, T.-W. Fang, and S. Srivastava, "IDEASSat: A 3U CubeSat mission for ionospheric science," *Adv. Space Res.*, vol. 66, no. 1, pp. 116–134, Jul. 2020, doi: 10.1016/j.asr.2020.01.012.

[6] S. Wu, W. Chen, C. Cao, C. Zhang, and Z. Mu, "A multiple-CubeSat constellation for integrated Earth observation and marine/air traffic monitoring," *Adv. Space Res.*, vol. 67, no. 11, pp. 3712–3724, Jun. 2021, doi: 10.1016/j.asr.2020.04.025.

[7] Y. Yao, Z. Jiang, H. Zhang, and Y. Zhou, "On-board ship detection in micro-nano satellite based on deep learning and COTS component," *Remote Sens.*, vol. 11, no. 7, p. 762, Mar. 2019, doi: 10.3390/rs11070762.

[8] M. E. Grøtte, R. Birkeland, E. Honoré-Livermore, S. Bakken, J. L. Garrett, E. F. Prentice, F. Sigernes, M. Orlandić, and J. T. Gravdahl, "Ocean color hyperspectral remote sensing with high resolution and low latency—The HYPSO-1 CubeSat mission," *IEEE Trans. Geosci. Remote Sens.*, vol. 60, 2022, Art. no. 1000619, doi: 10.1109/TGRS.2021.3080175.

[9] M. Azami, N. Orger, V. Schulz, T. Oshiro, and M. Cho, "Earth observation mission of a 6U CubeSat with a 5-meter resolution for wildfire image classification using convolution neural network approach," *Remote Sens.*, vol. 14, no. 8, p. 1874, Apr. 2022, doi: 10.3390/rs14081874.

[10] L. Dyrud, J. Fentzke, G. Bust, B. Erlandson, S. Whitely, B. Bauer, S. Arnold, D. Selva, K. Cahoy, R. Bishop, W. Wiscombe, S. Lorentz, S. Slagowski, B. Gunter, and K. Trenberth, "GEOScan: A global, real-time geoscience facility," in *Proc. IEEE Aerosp. Conf.*, Mar. 2013, pp. 1–13, doi: 10.1109/AERO.2013.6497141.

[11] D.-H. Cho, W.-S. Choi, M.-K. Kim, J.-H. Kim, E. Sim, and H.-D. Kim, "High-resolution image and video CubeSat (HiREV): Development of space technology test platform using a low-cost CubeSat platform," *Int. J. Aerosp. Eng.*, vol. 2019, May 2019, Art. no. 8916416, doi: 10.1155/2019/8916416.

[12] A. Poghosyan and A. Golkar, "CubeSat evolution: Analyzing CubeSat capabilities for conducting science missions," *Prog. Aerosp. Sci.*, vol. 88, pp. 59–83, Jan. 2017.

[13] J. Willis, P. Walton, D. Wilde, and D. Long, "Miniaturized solutions for CubeSat servicing and safety requirements," *IEEE J. Miniaturization Air Space Syst.*, vol. 1, no. 1, pp. 3–9, Jun. 2020, doi: 10.1109/TGRS.2019.2954807.

[14] R. De, M. P. Abegaonkar, and A. Basu, "Enabling science with CubeSats—Trends and prospects," *IEEE J. Miniaturization Air Space Syst.*, vol. 3, no. 4, pp. 221–231, Dec. 2022, doi: 10.1109/JMASS.2022.3209897.

[15] T. F. C. Leao, V. Mooney-Chopin, C. W. Trueman, and S. Gleason, "Design and implementation of a diplexer and a dual-band VHF/UHF antenna for nanosatellites," *IEEE Antennas Wireless Propag. Lett.*, vol. 12, pp. 1098–1101, 2013, doi: 10.1109/LAWP.2013.2280454.

[16] Y. Rahmat-Samii, V. Manohar, and J. M. Kovitz, "For satellites, think small, dream big: A review of recent antenna developments for CubeSats," *IEEE Antennas Propag. Mag.*, vol. 59, no. 2, pp. 22–30, Apr. 2017, doi: 10.1109/MAP.2017.2655582.

[17] S. Gao, K. Clark, M. Unwin, J. Zackrisson, W. A. Shiroma, J. M. Akagi, K. Maynard, and P. Garner, "Antennas for modern small satellites," *IEEE Antennas Propag. Mag.*, vol. 51, no. 4, pp. 40–56, Aug. 2009, doi: 10.1109/MAP.2009.5338683.

[18] W. Hasbi, M. Mukhayadi, and U. Renner, "The impact of space-based AIS antenna orientation on in-orbit AIS detection performance," *Appl. Sci.*, vol. 9, no. 16, p. 3319, Aug. 2019, doi: 10.3390/app9163319.

[19] X. Zhang, F. Sun, G. Zhang, and L. Hou, "Compact UHF/VHF monopole antennas for CubeSats applications," *IEEE Access*, vol. 8, pp. 133360–133366, 2020, doi: 10.1109/ACCESS.2020.3008540.

[20] K. Schraml, A. Narbudowicz, S. Chalermwisutkul, D. Heberling, and M. J. Ammann, "Easy-to-deploy LC-loaded dipole and monopole antennas for CubeSat," in *Proc. 11th Eur. Conf. Antennas Propag. (EUCAP)*, Mar. 2017, pp. 2303–2306, doi: 10.23919/EuCAP.2017.7928135.

[21] *World's Largest Database of Nanosatellites*. Accessed: Jan. 10, 2023. [Online]. Available: https://www.nanosats.eu/#figures

[22] S. Abulgasem, F. Tubbal, R. Raad, P. I. Theoharis, S. Lu, and S. Iranmanesh, "Antenna designs for CubeSats: A review," *IEEE Access*, vol. 9, pp. 45289–45324, 2021, doi: 10.1109/ACCESS.2021.3066632.

[23] H. H. Abdullah, A. Elboushi, A. E. Gohar, and E. A. Abdallah, "An improved S-band CubeSat communication subsystem design and implementation," *IEEE Access*, vol. 9, pp. 45123–45136, 2021, doi: 10.1109/ACCESS.2021.3066464.

[24] M. J. Veljovic and A. K. Skrivervik, "Aperture-coupled low-profile wideband patch antennas for CubeSat," *IEEE Trans. Antennas Propag.*, vol. 67, no. 5, pp. 3439–3444, May 2019, doi: 10.1109/TAP.2019.2900428.

[25] E. Pittella, S. Pisa, and A. Nascetti, "Reconfigurable S-band patch antenna radiation patterns for satellite missions," in *Proc. 5th IEEE Int. Workshop Metrol. Aerosp. (MetroAeroSpace)*, Jun. 2018, pp. 651–656, doi: 10.1109/MetroAeroSpace.2018.8453576.

[26] A. D. Johnson, V. Manohar, S. B. Venkatakrishnan, and J. L. Volakis, "Low-cost S-band reconfigurable monopole/patch antenna for CubeSats," *IEEE Open J. Antennas Propag.*, vol. 1, pp. 598–603, 2020, doi: 10.1109/OJAP.2020.3034051.

[27] J. F. Munoz-Martin, L. F. Capon, J. A. Ruiz-de-Azua, and A. Camps, "The flexible microwave payload-2: A SDR-based GNSS-reflectometer and L-band radiometer for CubeSats," *IEEE J. Sel. Topics Appl. Earth Observ. Remote Sens.*, vol. 13, pp. 1298–1311, Mar. 2020, doi: 10.1109/JSTARS.2020.2977959.

[28] Y. Yao, S. Liao, J. Wang, and K. Xue, "A new patch antenna designed for CubeSat: Dual feed, LS dual-band stacked, and circularly polarized," *IEEE Antennas Propag. Mag.*, vol. 58, no. 3, pp. 16–21, Jun. 2016, doi: 10.1109/MAP.2016.2541601.

[29] M. J. Veljovic and A. K. Skrivervik, "Patch antenna system for CubeSats in L band," in *Proc. 13th Eur. Conf. Antennas Propag. (EuCAP)*, Krakow, Poland, Mar./Apr. 2019, pp. 1–5.

[30] B. Alshammari, K. Alrushud, M. Kuznetcov, Y. Li, and S. K. Podilchak, "Dual-band dually-polarized compact folded-shorted patch array for small satellites," in *Proc. IEEE Int. Symp. Antennas Propag. USNC-URSI Radio Sci. Meeting (APS/URSI)*, Singap., Dec. 2021, pp. 707–708, doi: 10.1109/APS/URSI47566.2021.9703829.

[31] S. Gao, Y. Rahmat-Samii, R. E. Hodges, and X. X. Yang, "Advanced antennas for small satellites," *Proc. IEEE*, vol. 106, no. 3, pp. 391–403, Mar. 2018, doi: 10.1109/JPROC.2018.2804664.

[32] S. Liu, P. I. Theoharis, R. Raad, F. Tubbal, A. Theoharis, S. Iranmanesh, S. Abulgasem, M. U. A. Khan, and L. Matekovits, "A survey on CubeSat missions and their antenna designs," *Electronics*, vol. 11, no. 13, p. 2021, Jun. 2022, doi: 10.3390/electronics11132021.

[33] J. Costantine, Y. Tawk, I. Maqueda, M. Sakovsky, G. Olson, S. Pellegrino, and C. G. Christodoulou, "UHF deployable helical antennas for CubeSats," *IEEE Trans. Antennas Propag.*, vol. 64, no. 9, pp. 3752–3759, Sep. 2016, doi: 10.1109/TAP.2016.2583058.

[34] L. Fernandez, M. Sobrino, J. A. Ruiz-de-Azua, A. Calveras, and A. Camps, "Design of a deployable helix antenna at L-band for a 1-unit CubeSat: From theoretical analysis to flight model results," *Sensors*, vol. 22, no. 10, p. 3633, May 2022, doi: 10.3390/s22103633.

[35] L. Fernandez, M. Sobrino, O. Milian, A. Aguilella, A. Solanellas, M. Badia, J. F. Munoz-Martin, J. A. Ruiz-de-Azua, M. Sureda, and A. Camps, "Deployment mechanism for a L-band helix antenna in 1-unit CubeSat," *Acta Astronautica*, vol. 196, pp. 394–399, Jul. 2022, doi: 10.1016/j.actaastro.2020.09.005.

[36] M. Sureda, M. Sobrino, O. Millan, A. Aguilella, A. Solanellas, M. Badia, J. F. Munoz-Martin, L. Fernandez, J. A. Ruiz-De-Azua, and A. Camps, "Design and testing of a helix antenna deployment system for a 1U CubeSat," *IEEE Access*, vol. 9, pp. 66103–66114, 2021, doi: 10.1109/ACCESS.2021.3075660.

[37] A. Takacs, H. Aubert, D. Belot, and H. Diez, "Miniaturization of compact quadrifilar helix antennas for telemetry, tracking and command applications," *Prog. Electromagn. Res. C*, vol. 60, pp. 125–136, 2015, doi: 10.2528/PIERC15072606.

[38] M. Sakovsky, S. Pellegrino, and J. Costantine, "Rapid design of deployable antennas for CubeSats: A tool to help designers compare and select antenna topologies," *IEEE Antennas Propag. Mag.*, vol. 59, no. 2, pp. 50–58, Apr. 2017, doi: 10.1109/MAP.2017.2655531.

[39] G. P. Knott, C. Wu, and A. Viquerat, "Deployable bistable composite helical antennas for small satellite applications," in *Proc. AIAA Scitech Forum*, San Diego, CA, USA, Jan. 2019, pp. 1–10, doi: 10.2514/6.2019-1260.

[40] S. Rogers, "Phoenix: A CubeSat mission to study the impact of urban heat islands within the U.S.," presented at the 34th Annu. SmallSat [Virtual Conf.], 2020. [Online]. Available: https://digitalcommons.usu.edu/cgi/viewcontent.cgi?article=4614&context=smallsat

[41] B. Schoch, S. Chartier, U. Mohr, M. Koller, S. Klinkner, and I. Kallfass, "Towards a CubeSat mission for a wideband data transmission in E-band," in *Proc. IEEE Space Hardw. Radio Conf. (SHaRC)*, San Antonio, TX, USA, Jan. 2020, pp. 16–19, doi: 10.1109/SHaRC47220.2020.9034007.

[42] M. R. Mughal et al., "Aalto-1, multi-payload CubeSat: In-orbit results and lessons learned," *Acta Astronautica*, vol. 187, pp. 557–568, Oct. 2021, doi: 10.1016/j.actaastro.2020.11.044.

[43] J. Praks, A. Kestila, M. Hallikainen, H. Saari, J. Antila, P. Janhunen, and R. Vainio, "Aalto-1—An experimental nanosatellite for hyperspectral remote sensing," in *Proc. IEEE Int. Geosci. Remote Sens. Symp.*, Vancouver, BC, Canada, Jul. 2011, pp. 4367–4370, doi: 10.1109/IGARSS.2011.6050199.

[44] J. A. Fraire, G. Nies, H. Hermanns, K. Bay, and M. Bisgaard, "Battery-aware contact plan design for LEO satellite constellations: The ulloriaq case study," in *Proc. IEEE Global Commun. Conf. (GLOBECOM)*, Dec. 2018, pp. 1–7, doi: 10.1109/GLOCOM.2018.8647822.

[45] A. Perez, P. Fabregat, M. Badia, M. Sobrino, C. Molina, J. F. Munoz-Martin, L. Fernandez, L. Rayon, and J. Ramos, "RITA: Requirements and preliminary design of an L-band microwave radiometer, optical imager, and RFI detection payload for a 3U CubeSat," in *Proc. IEEE Int. Geosci. Remote Sens. Symp. (IGARSS)*, Sep. 2020, pp. 5986–5989, doi: 10.1109/IGARSS39084.2020.9324458.

[46] J. Praks, P Niemelä, A. Näsilä, A. Kestilä, N. Jovanovic, and B. Riwanto, "Miniature spectral imager in-orbit demonstration results from Aalto-1 nanosatellite mission," in *Proc. IEEE Int. Geosci. Remote Sens. Symp. (IGARSS)*, Jul. 2018, pp. 1986–1989, doi: 10.1109/IGARSS.2018.8517658.

[47] C. M. Pong and M. W. Smith, "Camera modeling, centroiding performance, and geometric camera calibration on ASTERIA," in *Proc. IEEE Aerosp. Conf.*, Mar. 2019, pp. 1–17, doi: 10.1109/AERO.2019.8741842.

[48] A. D. Santangelo and K. M. Crosby, "The CaNOP CubeSat mission: Updates, results and applications," in *Proc. ASCEND*, Nov. 2020, doi: 10.2514/6.2020-4176.

[49] M. Kubicka, R. Zeif, M. Henkel, and A. J. Hörmer, "Thermal vacuum tests for the ESA's OPS-SAT mission," *e & i Elektrotechnik und Informationstechnik*, vol. 139, no. 1, pp. 16–24, Feb. 2022, doi: 10.1007/s00502-022-00990-w.

[50] A. Nascetti, E. Pittella, P. Teofilatto, and S. Pisa, "High-gain S-band patch antenna system for earth-observation CubeSat satellites," *IEEE Antennas Wireless Propag. Lett.*, vol. 14, pp. 434–437, 2015, doi: 10.1109/LAWP.2014.2366791.

[51] N. Meirambekuly, A. A. Temirbayev, Z. Z. Zhanabaev, B. A. Karibayev, T. A. Namazbayev, B. A. Khaniyev, and A. K. Khaniyeva, "Dual-band optical imaging system-integrated patch antenna based on anisotropic fractal for Earth-observation CubeSats," *Ain Shams Eng. J.*, vol. 13, no. 2, Mar. 2022, Art. no. 101560, doi: 10.1016/j.asej.2021.07.010.

[52] C. A. Balanis, "Traveling wave and broadband antennas," in *Antenna Theory, Analysis and Design*, 3rd ed. Hoboken, NJ, USA: Wiley, 2005, ch. 10, sec. 10.3.1, pp. 566–573. https://ia601200.us.archive.org/35/items/AntennaTheoryAnalysisAndDesign3rdEd/Antenna%20Theory%20Analysis%20and%20Design%203rd%20ed.pdf
[53] Satsearch. *CubeSat Cameras and Optical Payloads for Small Satellites on the Global Marketplace*. Accessed: Nov. 15, 2022. [Online]. Available: https://blog.satsearch.co/2020-03-25-optical-payloads-for-small-satellites-a-sector-overview
[54] Simera Sense. *A New Standard For Earth Observation*. Accessed: Nov. 15, 2022. [Online]. Available: https://simera-sense.com/cubesat-imager/
[55] M. Storch, T. Jarmer, M. Adam, and N. de Lange, "Systematic approach for remote sensing of historical conflict landscapes with UAV-based laserscanning," *Sensors*, vol. 22, no. 1, p. 217, Dec. 2021, doi: 10.3390/s22010217.
[56] GOMSpace. *High Performing Camera-System for Earth Observation Projects*. Accessed: Nov. 15, 2022. [Online]. Available: https://gomspace.com/shop/payloads/earth-observation.aspx
[57] C. Fonda and M. Zennaro, "Radio laboratory handbook," in *Antenna Measurements*. Feb. 2004, ch. 6. [Online]. Available: http://wireless.ictp.it/handbook/C6.pdf
[58] B. Li, "Axial ratio measurements of circularly polarised antennas based on polarisation rotation," *IET Microw., Antennas Propag.*, vol. 12, no. 15, pp. 2379–2382, Sep. 2018, doi: 10.1049/iet-map.2018.5421.

NURSULTAN MEIRAMBEKULY was born in Turkistan, Kazakhstan, in January 1994. He received the master's degree in technology from Al-Farabi KazNU, in 2018, where he is currently pursuing the Ph.D. degree. He took part in several research projects, including the developing of the first Kazakhstani nanosatellites. His research interests include antennas, small spacecrafts, telecommunications, and 3-D modeling.

BEIBIT A. KARIBAYEV was born in Kyzylorda, Kazakhstan, in April 1990. He received the master's degree in physics and astronomy from Al-Farabi KazNU, in 2013, where he is currently pursuing the Ph.D. degree with the Department of Solid State Physics and Nonlinear Physics. He is currently a Research Fellow with the Institute of Experimental and Theoretical Physics. He is engaged in research of antennas of fractal shapes, development a new type of antennas with multiband, and broadband properties.

TIMUR A. NAMAZBAYEV was born in Almaty, Kazakhstan, in August 1991. He received the master's degree in engineering from Al-Farabi KazNU, in 2015. He is currently a Research Fellow with the Institute of Experimental and Theoretical Physics. He is engaged in computer modeling, development of devices with multiband, and broadband properties.

GULAMA-GARIP ALISHER E. IBRAYEV was born in West-Kazakhstan, Kazakhstan, in June 1992. He received the Ph.D. degree in mechanical engineering from Al-Farabi KazNU, Kazakhstan, in 2022. He did an internship with Keele University, under the guidance of Prof. J. Kaplunov from Florida Atlantic University and Prof. I. Elishakoff. He is currently a Senior Lecturer with Al-Farabi KazNU. He took part in many research projects, including the launch of the first Kazakh nanosatellite. His research interests include space engineering, nonlinear vibrations, and control theory.

SABYR O. ORYNBASSAR was born in Shymkent, Kazakhstan, in September 1996. He received master's degree in radio engineering, electronics, and telecommunications from Al-Farabi KazNU, Kazakstan, in 2020. He is currently the Head of the Laboratory with the International Taraz Innovation Institute. His research and professional interests include design of printed circuit boards, circuit engineering, and electrical engineering.

SAMSONENKO ANATOLIY IVANOVICH was born in Almaty, Kazakhstan, in 1962. He received the B.S. degree in radio engineering from the Almaty Power Engineering Institute, Kazakhstan, in 1988. He is currently a Leading Researcher with the Institute of Space Technique and Technology. His research interests include space engineering, antenna systems, and energy power systems of spacecrafts.

AMIRKHAN A. TEMIRBAYEV was born in Tashkent, Uzbekistan, in April 1986. He received the Ph.D. degree in physics from Al-Farabi KazNU, Kazakhstan, in 2012. He is currently the General Director of the Cluster of Engineering and High Technologies, Al-Farabi KazNU. He is involved in the design of a KazNU's nanosatellites. He repeatedly passed scientific training in leading centers in Germany, Japan, and Holland. His research interests include nanosatellites, antenna systems for CubeSats, and STEM education.